Quaternary and pentanar mesoporous bioactive glass nanoparticles as novel nanocarriers for gallic acid: characterisation, drug release and antibacterial activity

Andrada-Ioana Damian-Buda[a], Qaisar Nawaz[a], Irem Ünalan[a], Ana M. Beltrán[b], Aldo R. Boccaccini[a,*]

[a] Institute of Biomaterials, Department of Materials Science and Engineering, University of Erlangen–Nuremberg, Cauerstraße 6, 91058 Erlangen, Germany

[b] Departamento de Ingeniería y Ciencia de Los Materiales y Del Transporte, Escuela Politécnica Superior, University of Seville, 41011 Seville, Spain

* corresponding author: aldo.boccaccini@fau.de (Aldo R. Boccaccini)

Abstract: Recently, mesoporous bioactive glass nanoparticles (MBGNs) have gained considerable attention as multifunctional platforms for simultaneously releasing ions and phytotherapeutic compounds. Thus, in the first part of this study, MBGNs based on 53SiO_2-4P_2O_5-20CaO-23Na_2O (wt %) (S53P4) composition were synthesized by a microemulsion assisted sol-gel method. More precisely, P_2O_5 was substituted with B_2O_3 and Na_2O with MgO and/or ZnO. For B containing MBGNs all ions were successfully incorporated into the borosilicate structure without inducing crystallisation. In contrast, for S53P4 a poorly crystalline hydroxyapatite phase was identified. All MBGNs had a typical spherical shape with an internal radial network of mesopores. Additionally, for S53P4 a second fraction of particles with a smaller size and compact core was observed. Secondly, the feasibility of MBGNs as nanocarriers for gallic acid (GA) was evaluated. All drug-loaded samples showed a similar *in vitro* release profile which can be divided

into three main phases: burst release, slow release and sustained release. Among the different compositions, S53P4 exhibited the highest cumulative release, whereas B and Mg containing particles exhibited the opposite. The presence of Zn in the MBGN compositions improved their antibacterial effect against both *E. coli* and *S. aureus*. Moreover, it was shown that depending on the MBGNs' composition, the antibacterial activity of GA loaded MBGNs can be enhanced. Thus, the results proved that MBGNs can be used as controlled drug delivery system and, by tailoring the composition, a synergistic antibacterial effect can be achieved, considering that GA and biologically active ions are simultaneously released.

Keywords: *mesoporous bioactive glass nanoparticles, control release, gallic acid, antibacterial effect*

1. Introduction

Worldwide, one out of ten people had diabetes mellitus in 2020 and this number is expected to increase by over 45% until 2040 [1]. Among different complications associated with this disease, food ulcers stand out due to their high prevalence, affecting over 35% of diabetic patients at least once during their lifetime [2]. Moreover, half of the diabetic wounds are prone to life-threatening bacterial infection [3]. As a result of poor wound care management, every 20 seconds a lower diabetic limb is amputated [4, 5]. To prevent the worsening of the existing ulcers, traditional therapies such as gauzes, bandages, or topical ointments are currently used [6]. However, they easily adhere to the wound surface, triggering pain and trauma when removed [7, 8]. To enhance the

regeneration process and to promote specific cellular pathways, advanced wound dressings containing growth factors, drugs or nanoparticles have been developed [7, 9].

Nowadays bioactive glass (BG) is widely used as synthetic bone graft due to its ability to from a strong interfacial bond with the surrounding tissue [10]. At the same time, different compositions of BGs have shown immense potential for soft tissue engineering applications by promoting angiogenesis, epithelial cell migration, and fibroblast proliferation [11–13]. For instance, 13-93B3 borate-based bioactive glass microfibers (Mirragen® with composition: $53B_2O_3$-$6Na_2O$-$12K_2O$-5MgO-20CaO-$4P_2O_5$ wt%) were approved by the FDA in 2016 for treating acute and chronic wounds. To further increase the reactivity of the material and induce a higher regeneration rate [14], mesoporous bioactive glass nanoparticles (MBGNs) are gaining increasing attention. In this "Era of Innovation" [15], extensive research is focused on tailoring the MBGNs' composition to achieve specific therapeutic effects (angiogenesis, antibacterial, anti-inflammatory and/or anti-oxidant effect, etc.) [16–18].

Although present only in small amounts in the body, boron is an essential trace element that plays a pivotal role in regulating the biochemical processes at cellular level. It has been previously demonstrated that B^{3+} stimulates the secretion and the overexpression of different growth factors [19]. Thus, the angiogenesis process is activated [20], and proliferation and migration of fibroblasts and keratinocytes are promoted [21]. The same positive modulation of angiogenesis and cell migration has been reported for Mg^{2+} and Zn^{2+} [22]. Moreover, Yu et al. [23] showed that the simultaneous release of Mg^{2+} and Si^{4+} accelerates the maturation of the extracellular matrix (ECM) and improves neovascularization. During this process, it is of utmost importance to prevent the development of serious infections at the wounded site. Thus, Zn^{2+}, known for its

strong antibacterial effect [24, 25], could be incorporated into the MBGN composition. At the same time, the presence of Zn^{2+} should increase the gene expression of different proteins with anti-inflammatory activities [26].

In addition to their outstanding biological properties, MBGNs have a controlled mesostructure, narrow pore size distribution, and high specific surface area [27, 28]. These unique textural properties can be exploited to load and achieve sustained release of therapeutic drugs and growth factors [29]. As a result, the drug's side effects and the dosing frequency are reduced, while the efficiency and availability of the drug increase [30]. To effectively treat wound infections, several types of antibiotics are frequently used. However, the improper administration of antibiotics has led to the development of antibiotic-resistant strains which are hardly destroyed by conventional treatments [31]. One novel approach that can be used to overcome this challenge is to synergistically combine phytotherapeutic agents and BGs releasing antibacterial ions [32–34].

Gallic acid (GA) (3,4,5-trihydroxybenzoic acid) is a low molecular mass polyphenol compound usually found in pomegranate root bark, tea leaves, oak bark, gallnuts, and sumac [31]. It is a natural metabolite that has been recently investigated for wound healing applications due to its promising antioxidant properties [31, 35]. In addition, GA has powerful antibacterial activity, inducing irreversible membrane changes in both Gram-negative and Gram-positive bacterial strains [36]. Lee et al. [37] proved that GA functionalized ZnO nanoparticles had an antibacterial effect against *E. coli* compared to simple ZnO. In another study, Yang et al. [38] investigated the effect of GA on the wound healing process in normal and diabetic conditions. In both environments, the results revealed that GA is directly involved in the upregulation of antioxidant genes, while accelerating the migration of fibroblasts and keratinocytes.

In this study, we aim to develop different types of quaternary and pentanar MBGNs as nanocarriers for GA. MBGNs were synthetised in the S53P4 ($53SiO_2$-$4P_2O_5$-20CaO-$23Na_2O$ wt %) compositional system. Despite being approved for treating bone infection, S53P4 has been poorly investigated for wound care applications in soft tissues [13]. This might be due to the high network connectivity of this silicate-based BG, which leads to slow degradation rates [10]. One strategy that can be applied to increase the solubility and stimulate the regeneration process, is to incorporate B_2O_3 in the structure [13, 39]. Thus, P_2O_5 was fully substituted with B_2O_3. Moreover, in the commercially available S53P4 BG, Na_2O is added to lower the melting temperature of the precursors' mixture [40]. In contrast, the microemulsion assisted sol-gel method used in this work does not require high processing temperatures [41]. Na_2O was completely substituted with ZnO and/or MgO to improve the MBGNs' therapeutic properties. Thus, one of the aims of this study was to highlight the influence of the composition on the structural and morphological characteristics of MBGNs. Considering the high loading capacities of mesoporous materials, MBGNs were further investigated as controlled drug delivery systems for GA. The effect of different types of MBGNs on the drug release profile has been highlighted. Finally, the antibacterial effect that results from the combined and simultaneous release of a natural compound (GA) and different antibacterial ions was evaluated.

2. Materials and methods

2.1 Materials

For the synthesis of MBGNs and GA loaded MBGNs, the following chemicals were used: cetyltrimethylammonium bromide (CTAB, $C_{19}H_{42}BrN$, >97%, Merck, Germany), ethyl acetate (EA, $C_4H_8O_2$, >99.5%, Merck, Germany), ammonia (NH_3, 28%, VWR International, France), tetraethyl orthosilicate (TEOS, 98%, Sigma Aldrich, Germany), ammonium phosphate dibasic ($(NH_4)_2HPO_4$, ≥98%, Sigma-Aldrich, Germany), boric acid (H_3BO_3, ≥99.5%, Sigma-Aldrich, Germany), calcium nitrate tetrahydrate ($Ca(NO_3)_2{\cdot}4H_2O$, 98.5%, VWR International, Belgium), sodium nitrate ($NaNO_3$, ≥99%, Sigma-Aldrich, Germany), magnesium nitrate hexahydrate ($Mg(NO_3)_2{\cdot}6H_2O$, 99%, Sigma-Aldrich, Germany), zinc nitrate hexahydrate ($Zn(NO_3)_2{\cdot}6H_2O$, ≥99%, Sigma-Aldrich, Germany), gallic acid ($C_7H_6O_5$, ≥98.0%, Sigma-Aldrich, Germany), absolute ethanol (EtOH, 99.8%, Alfa Aesar, Germany), ultrapure water (MilliQ) and Dulbecco's phosphate-buffered saline (DPBS, Thermo Fischer, Germany).

2.2 Synthesis of mesoporous bioactive glass nanoparticles

In this study, four different MBGN compositions (Table 1) have been synthesized using a modified microemulsion-assisted sol-gel method, as described previously [17, 42]. Briefly, 1.36 g of CTAB was dissolved in 65 ml MilliQ while stirring at 37°C for 30 minutes. Once the solution became clear, the temperature was switched off and 20 ml of ethyl acetate (EA) was dropwise added. After 30 minutes of stirring, 27 ml ammonium hydroxide was added until a pH of 9.5 was reached. Then, 8 ml of TEOS was slowly poured to the previously obtained solution. In this mixture, 0.304 g H_3BO_3, previously dissolved in minimum amount of MilliQ, was added simultaneously with ammonium

hydroxide to maintain the pH at 9.5. Within a time gap of 30 minutes, 3.403 g $Ca(NO_3)_2 \cdot 4H_2O$ and $Mg(NO_3)_2 \cdot 6H_2O$ were added. Following 4 hours of swirling, the precipitate was collected by centrifugation at 4800/5min (Centrifuge 5430R, Eppendorf, Germany) and washed two times with MilliQ and EtOH. The collected particles were dried overnight at 60°C and then calcinated at 600℃ for 3 hours (heating rate of 2°C/min). For the S53P4, B+Zn and B+Mg+Zn compositions, the same experimental steps were followed, with the amounts of precursors determined from the nominal compositions.

Table 1

Nominal compositions of synthesized MBGNs (%wt)

Symbol	SiO_2	P_2O_5	B_2O_3	Na_2O	CaO	MgO	ZnO
S53P4	53	4	-	23	20	-	-
B+Mg	53	-	4	-	20	23	-
B+Zn	53	-	4	-	20	-	23
B+Mg+Zn	53	-	4	-	20	11.5	11.5

2.3 Preparation of gallic acid loaded mesoporous bioactive glass nanoparticles

GA solutions of various concentrations (20 µg/ml, 50 µg/ml, 70 µg/ml, and 100 µg/ml) were prepared by dissolving the required amount of drug in DPBS for 30 minutes in the absence of light. Then, 0.2 g of MBGNs were dispersed in 20 ml GA solution and stirred for different times (3h, 5h and 7h). Subsequently, the suspension was centrifuged at 3000 rpm for 5 minutes. The GA loaded MBGNs were dried under the fume hood for 48h, while the supernatant was kept for further studies. For GA loaded MBGNs (GA-

MBGNs) the following notations were used: GA-S53P4, GA-B+Mg, GA-B+Zn and GA-B+Mg+Zn.

2.4 Physicochemical characterisation of mesoporous bioactive glass nanoparticles before and after gallic acid loading

MBGNs' crystalline structure was assessed with a X-ray diffractometer (MiniFlex 600, Rigaku) equipped with a Cu Kα radiation source. The samples were scanned within the 5° - 65° 2θ angle range, with a step size of 0.015° and a speed of 1.5°/min. The nature of the bonds and the functional groups present in MBGNs and GA-MBGNs were evaluated by attenuated total reflection Fourier-transform infrared (ATR-FTIR) spectroscopy (RAnity-1S, Shimadzu, Duisburg, Germany). The spectra were recorded in absorbance mode between 4000 and 400 cm^{-1}, with a resolution of 4 cm^{-1} and 42 scans. The morphology of the MBGNs was investigated with a field emission scanning electron microscope (FE-SEM, LEO 435VP, Auriga, Carl Zeiss™, Germany). The collected images were further processed in ImageJ software (NIH, USA) to determine the average diameter and to plot the diameter density distribution. The internal pore structure and elemental composition were further investigated by transmission electron microscopy ((S)TEM) and Energy-dispersive X-ray spectroscopy (EDX) with Talos F200X system (ThermoFisher Scientific, Waltham, MA, USA).

2.5 Gallic acid loading efficiency and in vitro release study

The drug loading efficiency and the amount of drug released were determined by UV–VIS spectrophotometry (Specord 40, Analytic Jena, Germany). First, the standard calibration curve was plotted, with the measurements being recorded at 259 nm where GA has its characteristic peak [43]. To determine the MBGNs' loading efficiency (LE),

the absorbance of the GA solutions was measured before and after the loading process, according to equation:

$$LE(\%) = \frac{c_0 - c_r}{c_0} \times 100 \quad (1)$$

where c_0 is the initial concentration of GA and c_r is the concentration of GA in the collected supernatant after loading.

The optimized loaded MBGNs were further used for the GA release study. More precisely, 100 mg of GA-MBGNs were immersed in 5 ml of DPBS and the samples were kept in a shaking incubator at 90 rpm and 37℃. After predetermined time points (1h, 2h, 3h, 4h, 5h, 6h, 24h, 48h, 72h, 168h, 192h, 216h and 240h) the samples were centrifugated at 2500 rpm for 5 min. 2 ml of supernatant were withdrawn and replaced with 2 ml of fresh DPBS. The GA concentration in the collected supernatant was determined and further used to find the cumulative GA release (CR_t) according to the following equation:

$$CR_t\ (\%) = \frac{V_W}{V_t} \times CR_{t-1} + R_t \quad (2)$$

where CR_t is the cumulative release at time t, V_w is the volume withdrawn, V_t is the total volume of DPBS, CR_{t-1} is the cumulative release at time $t-1$ and R_t is the amount released at time t.

2.6 Antibacterial test

The antibacterial activity of MBGNs and GA loaded MBGNs against *S. aureus* (Gram-positive) and *E. coli* (Gram-negative) was evaluated by turbidity assessment [44, 45]. Prior to the experiment, both bacteria strains were grown in lysogeny broth (LB, Luria/Miller) at 37°C for 24 h. The optical density (OD) of the bacteria suspension was adjusted to 0.015 (~1×10^7 colony forming units/ml) at 600 nm with a spectrophotometer (Thermo Scientific GENESYS 30, Germany). MBGNs powders were sterilized for 2 h

under UV light and 15 mg of each composition was incubated in 15 ml of LB medium. After 24 h of continuous shaking incubation at 37°C, the elution extracts were collected. 20 μl of bacterial suspension was added in 2 mL elution extract and the samples were incubated at 37°C for 3h, 6h and 24h. The relative bacteria viability was calculated with the following equation:

$$Relative\ bacterial\ viability\ (\%) = \frac{OD_{sample} - OD_{blank}}{OD_{control} - OD_{blank}} \times 100 \quad (3)$$

2.7 Statistical analysis

All the experiments were performed in five replicates. The results are presented as the mean value ± standard deviation (SD). Additionally, mean differences were compared with one-way ANOVA and post hoc Bonferroni test provided by Origin 2021 software (OriginLab, Northampton, MA, USA). The intervals of confidence were denoted with * $p<0.05$, ** $p<0.01$ and *** $p<0.001$.

3. Results and discussions

3.1 Physicochemical characterisation of mesoporous bioactive glass nanoparticles

X-Ray diffraction analysis was performed to assess the degree of crystallinity of sintered MBGNs. For all compositions, the diffraction patterns (Fig. 1a) presented a broad halo between $2\theta=15°$ and $2\theta=30°$, characteristic of amorphous silicate bioactive glass [46, 47]. Additionally, in the S53P4 sample, a poorly crystalline hydroxyapatite (HA) (JCPDS 084-1998) phase was identified, whereas for the B doped MBGNs no diffraction peaks were recorded. These results might suggest that boron is incorporated homogeneously in the MBGNs' structure [47].

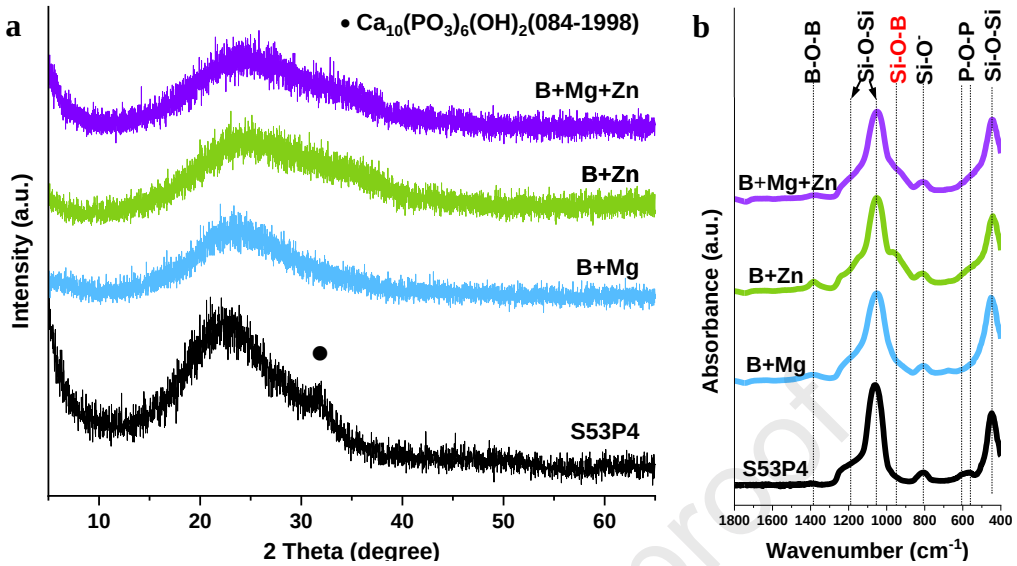

Fig. 1 (a) XRD patterns and (b) ATR-FTIR spectra of MBGNs.

The BG network was further investigated by ATR-FTIR (Fig. 1b). In all four spectra specific bands for the silicate network were highlighted. More precisely, the band located at 1058 cm^{-1} together with the shoulder at 1185 cm^{-1} could be attributed to symmetric Si-O-Si stretching vibration [48]. The peak at 445 cm^{-1} could correspond to Si-O-Si rocking vibration [34, 35]. The presence of Si-O-NBO asymmetric stretching band at 803 cm^{-1} confirmed the partial disruption of the silicate network due to the cations' incorporation into the network [34, 35]. In addition, in the S53P4 spectrum specific bands for O-P-O bending and stretching vibration of PO_4^{3-} groups in HA were identified at 560 cm^{-1} and 600 cm^{-1} [49]. In contrast, for B+Mg, B+Zn and B+Mg+Zn samples the peak at 1388 cm^{-1} could be identified with the B-O-B stretching vibration in BO_3 units, while the band at 932 cm^{-1} was attributed to the stretching frequency of Si-O-B [50]. These observations prove that S53P4 MBGNs contain P, while for the B doped compositions, B_2O_3 groups were integrated in the silicate network.

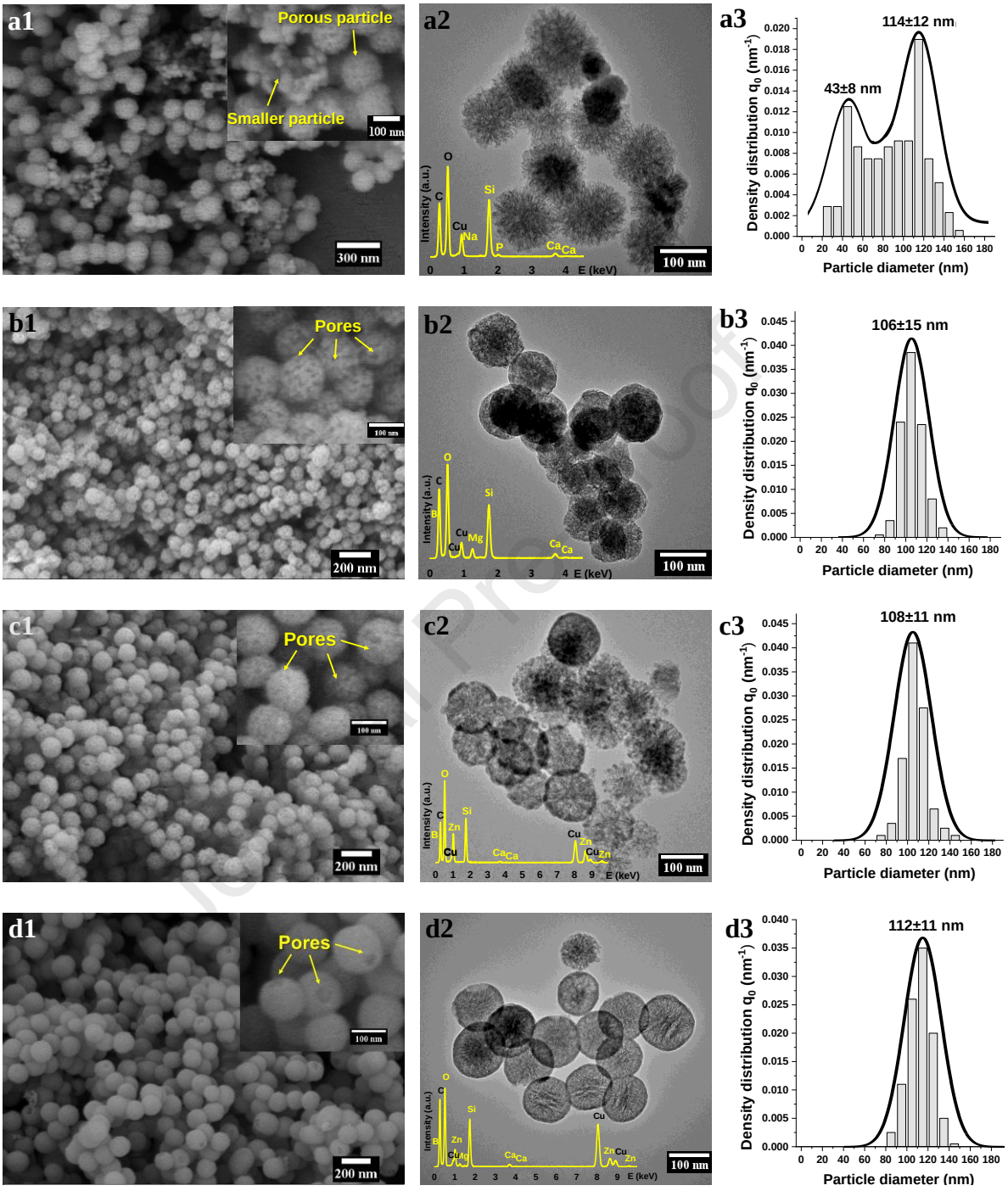

Fig. 2 SEM images of (a1) S53P4, (b1) B+Mg, (c1) B+Zn and (d1) B+Mg+Zn. TEM images and EDX spectra of (a2) S53P4, (b2) B+Mg, (c2) B+Zn and (d2) B+Mg+Zn. Numbered weighted density distribution for (a3) S53P4, (b3) B+Mg, (c3) B+Zn and (d3) B+Mg+Zn.

The morphology of MBGNs was investigated by SEM (Fig.2a1, b1, c1 and d1). For all four compositions, the particles had a similar spherical shape with a low tendency to form agglomerates. Moreover, on the surface of the particles, pores could be seen. These characteristics (shape, agglomeration and dimension) are specific for MBGNs synthetised by microemulsion assisted sol-gel method [17, 42, 51]. However, in the case of S53P4, a second fraction of particles with a smaller diameter and a smoother surface was identified. The number weighted particle size distribution (Fig. 2a3, b3, c3 and d3) for S53P4 showed a bimodal distribution, corresponding to the two fractions previously described. In contrast, B+Mg, B+Zn and B+Mg+Zn MBGNs had a narrower monomodal particle size distribution with similar average diameters between them and the larger S53P4 MBGNs. These observations were confirmed by TEM images where for S53P4 MBGNs the two families of particles were identified as: smaller compact particles and larger mesoporous particles. The bigger S53P4 particles had similar morphological characteristics with the B doped MBGNs, presenting an internal radial structure of slit-shape pores [42]. In addition, the EDX spectra confirmed the presence of all the elements characteristic for each corresponding composition. The distribution of elements in S53P4 MBGNs was further investigated. As it can be seen from Fig. 3, Ca and P are mainly present within the small particles, whereas the amount of Si is higher in the mesoporous particles compared to the compact particles. One possible explanation for this compositional and morphological difference comes from the microemulsion assisted sol-gel synthesis itself. It is known that due to the higher condensation rate of SiO_2 compared to the rate of absorption of ions in the network, not all the ions are included in the MBGNs structure [47]. As a result, the remaining Ca^{2+} and PO_4^{3-} ions could interact leading to the coprecipitation of HA as the pH of the solution is in the required pH range for HA

formation (between 9 and 12) [52]. Thus, it can be concluded that by substituting P_2O_5 with B_2O_3, one single fraction of particles with similar sizes was obtained.

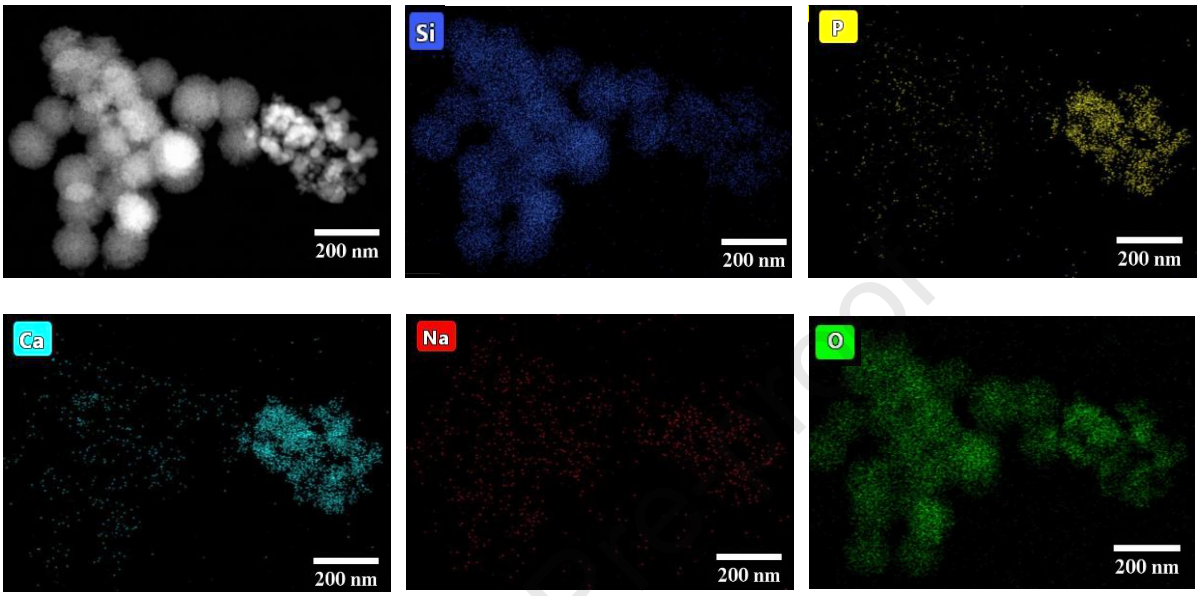

Fig. 3 STEM image with the corresponding EDX mapping of elements for S53P4 MBGNs.

3.2 Optimization of gallic acid loading process

The mesoporous internal structure of the previously presented MBGNs make them perfect candidates for the development of controlled drug delivery systems. Thus, GA was loaded into the mesopores via physical adsorption. To determine the optimal loading parameters, different loading times (3 h, 5h and 7h) and concentrations (20 µg/ml, 50 µg/ml, 70 µg/ml and 100 µg/ml) were studied for each composition (Fig. 4). For all GA concentrations and MBGNs' compositions, the maximum loading efficiency was achieved after 5 h. Thus, this time was further chosen as the optimal loading time. The increase of GA concentration from 20 µg/ml to 50 µg/ml and/or 70 µg/ml led to an increase of the drug loading efficiency. Above 70 µg/ml the loading efficiency was reduced which might be due to the GA supersaturation. For all GA concentrations, the

maximum LE for B+Mg was higher compared to the other compositions. It was previously proven that GA therapeutic dose for wound healing applications is 30 μm/ml [53]. Hence, for all compositions the loading time was 5 h and the GA concentration was adjusted to achieve the desired therapeutic concentration. More precisely, for B+Mg GA the optimal concentration used was 50 μg/ml (LE ~ 60%), while for the other compositions it was 70 μg/ml (LE ~ 43.5%).

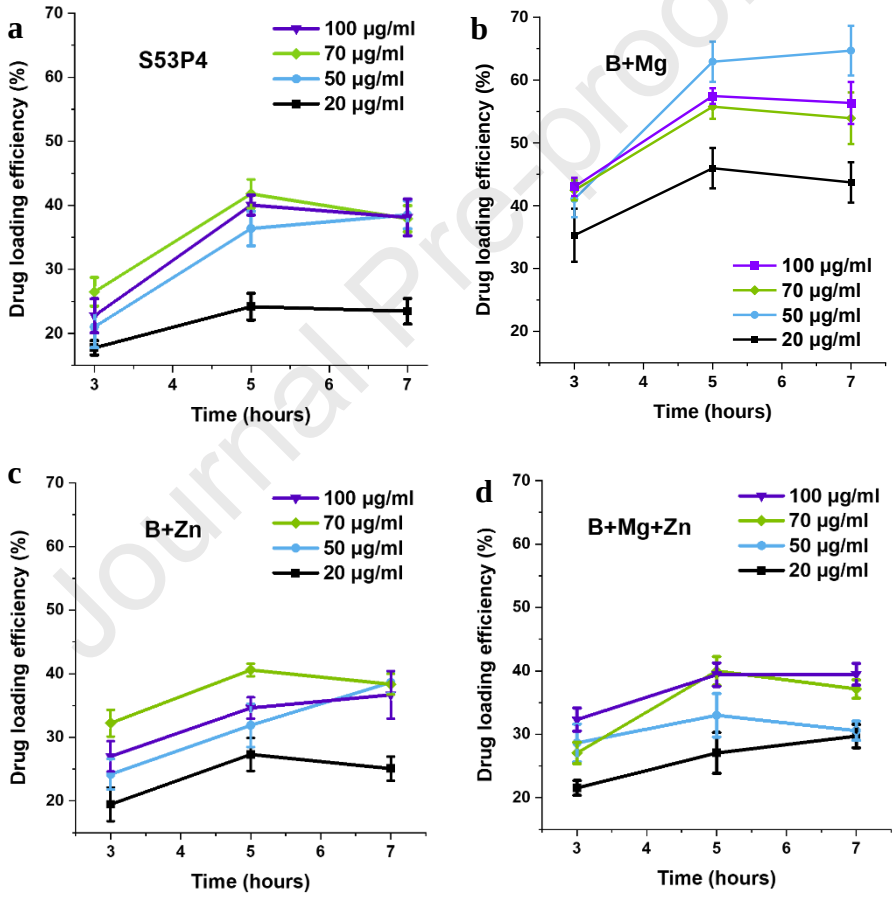

Fig. 4 Optimization of drug loading for (a) S53P4, (b) B+Mg, (c) B+Zn and (d) B+Mg+Zn MBGNs.

3.3 In vitro drug release study

One of the aims of controlled drug delivery systems is to achieve a constant drug concentration for long periods of time (sustained release). Thus, the release of GA from MBGNs was investigated. As shown in Fig. 5, for all compositions the cumulative release profile shows three main phases. In the first 3 h a high amount of drug is released from all types of MBGNs with the highest value achieved for GA-S53P4. This phase might be attributed to the drug molecules which are physically adsorbed on the surface of the particles and these molecules are the first ones to diffuse in the release medium. One possible explanation for the higher initial release for GA-S53P4 is the existence of two fractions of particles with different morphologies. In addition to the mesoporous particles identified also for B+Mg, B+Zn and B+Mg+Zn, the S53P4 sample also contains a fraction of small particles, which are less porous. This means that even though the concentration of drug loaded was the same in all the samples, the amount of drug entrapped between the particles might be higher for the S53P4 material. In the second phase (3 h – 24 h), similar releasing profiles were recorded for all compositions, but the release was slower compared to the first 3 h. This can be attributed to the drug which is physically incorporated inside the pores. After 24 h, a sustained, controlled and continuous drug release up to 10 days was achieved (Fig. 5b). This might be a result of the drug-mesopore wall interactions. At the pH at which the loading process was performed (7.4) the carboxyl group present in the GA structure is deprotonated [54]. Thus, the negatively charged group (COO^-) can chelate divalent cations present in the BG network (Ca^{2+}, Zn^{2+} and Mg^{2+}) and form coordinate bonds (Fig. 5c) [55]. Moreover, during the whole releasing process, the amount of drug release was higher for GA-B+Zn compared to GA-B+Mg and GA-B+Mg+Zn samples. In a previous study where the same B containing

compositions were obtained, it was shown that B+Zn MBGNs had a larger pore diameter compared to the other two [42]. More precisely, for MBGNs B+Mg MBGNs, the average pore diameter was 8.7 nm and the total pore volume was 1.25 cm^3/g, compared to 9.2 nm and 1.62 cm^3/g for B+Zn MBGNs, and 8.8 nm and 1.28 cm^3/g in for B+Mg+Zn MBGNs, respectively. Hence, it can be concluded that by increasing the pore diameter, GA was faster released. It should be mentioned that after 10 days the maximum cumulative release was approximately 70% for GA-S53P4, 60% for GA-Zn, 58% for GA-B+Zn and only 50% for GA-B+Mg. This means that the drug can be sustainably released for even longer periods of time, and the doses of administered drugs could be reduced. Thus, all the samples proved that MBGNs could be successfully used as drug nanocarriers for GA, tailoring the release kinetics depending on the final application. For instance, to treat chronic wounds which require longer regeneration times, GA-B+Mg MBGNs could be used as GA is more slowly released compared to GA-S53P4.

In a similar study, Nawaz et al. [32] highlighted the potential use of MBGNs as nanocarriers for the controlled and sustained release of silibinin. They proved that following a burst release in the first 24 h, the drug was continuously and sustained released for up to 20 days, most probably due to the interactions between the drug and MBGNs' surface. In another work conducted by Iarji et al. [56], GA was loaded into mesoporous silica nanoparticles (MSN). In the first 1.5 h approximately 80% of the drug was released, the cumulative release being above 90% after 2 weeks. The same behaviour was reported by Petrișor et al. [57] who investigated the effect of MSN pore size on the *in vitro* drug release. Compared to their findings, we achieved a slower and controlled GA release for all the compositions. In contrast to MSN, MBGNs have in their network

divalent cations which can form stable chelate compounds with GA which might explain the reduced cumulative release obtained in this study.

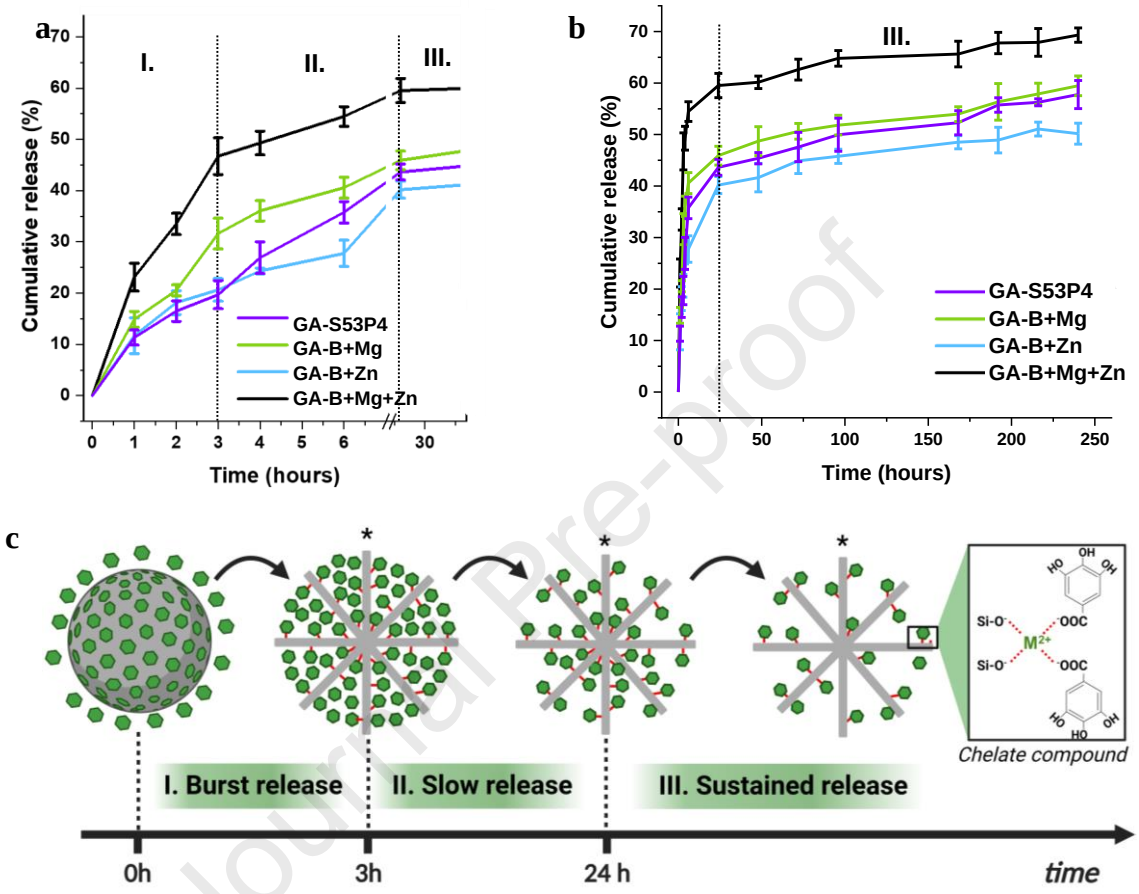

Fig. 5 *In vitro* drug release study up to (a) 30 h and (b) 10 days. (c) Schematic representation of the possible drug release mechanism (***** describes the possible internal structure of a particle in cross-section, see Fig. 2).

3.4 Antibacterial test

In order to ensure that MBGNs possess antibacterial properties, one current strategy involves incorporating into the BG network ions with antibacterial effect (Zn^{2+}, Ag^{+}, Cu^{2+}, etc. [24, 25]). At the same time, due to their unique textural properties, MBGNs can be loaded with a wide range of phytotherapeutic drugs. Among them, GA is

known to induce irreversible membrane changes in both Gram-positive *(S. aureus*) and Gram-negative (*E. coli*) bacterial strains, e.g. potentially exploiting synergy between the releasing ions and GA [36]. The previously presented strategies can be used together to further enhance the antibacterial effect. Therefore, one of the purposes of this study was to investigate the antibacterial effect of combining different ions with GA.

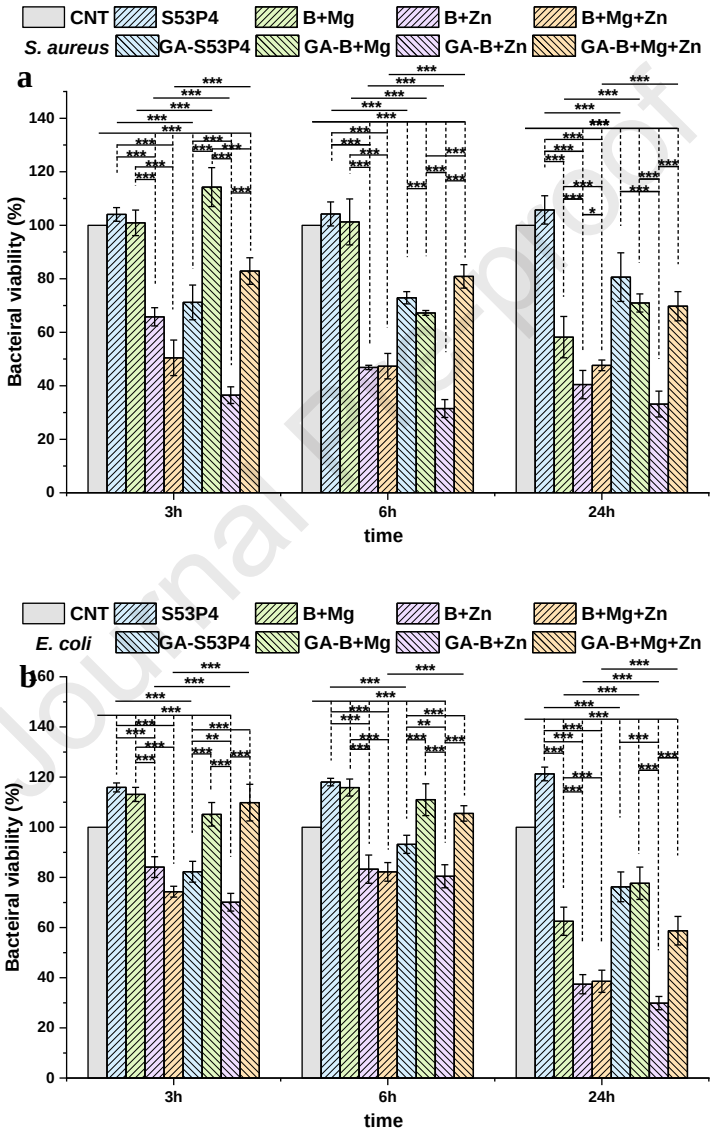

Fig. 6 *In vitro* antibacterial activity of MBGNs against (a) *E. coli* and (b) *S. aureus*.

he results of the turbidity test against *S. aureus* and *E. coli* are shown in Fig. 6. When the antibacterial assay was performed against *S. aureus*, for S53P4 and B+Mg no

significant differences were recorded compared to the control. However, the tests performed on *E. coli* revealed a slightly increase of the bacterial viability for both S53P4 and B+Mg. This might be because the S53P4 composition is less reactive than the standard 45S5 BG composition. Thus, the ionic concentration in the extract could have been below the minimum inhibitory concentration, in a range which favours bacteria growth. In contrast, for all the other samples similar behaviours were obtained on both bacterial strains. More precisely, for B+Zn and B+Mg+Zn both *E. coli* and *S. aureus* bacterial viabilities were constantly reduced as the inoculation time increased. This might be caused by the presence of Zn^{2+} in the glass structure which is known for its antibacterial activity [24]. For all drug loaded samples, the bacterial growth was significantly inhibited compared to the control at all testing times. However, in comparison with the unloaded samples, a stronger antibacterial effect was recorded only for GA-S53P4 and GA-B+Zn. The opposite situation was obtained for GA-Mg and GA-Mg+Zn. One possible explanation is the different drug release profiles of the different nanoparticle types. As it was previously presented, during the whole release study, GA-S53P4 and GA-B+Zn had a higher cumulative release compared to the other samples. As a result, a greater concentration of drug is present in the liquid, which could result in a stronger antibacterial action. In the case of GA-Mg and GA-Mg+Zn, the antibacterial activity is lower than or equal (for GA-Mg against *E. coli*) to the value obtained for the unloaded samples. This could be explained by the formation of stable coordinate bonds between the positively charged ions from the MBGNs and the (COO^-) group from GA. This strong interaction delays the release of ions and drugs. Furthermore, if the complex is released as a chelated compound, both components may lose their biological activity [58].

Even though all unloaded and loaded samples had a similar antibacterial effect on both strains of bacteria, there were small differences regarding the strength of the effect. For longer periods of testing time (24 h) the loaded samples were more efficient against *E. coli*, whereas for shorter times (3 h and 6 h) they showed a stronger antibacterial activity against *S. aureus. In vitro* studies showed that GA minimum inhibitory concentration for *S. aureus* and *E. coli* is 1750 µg/ml and 1500 µg/ml, respectively [59]. Compared to these values, we achieved antibacterial effects at lower GA doses (maximum amount of drug loaded 30 µg/ml). This suggests that the antibacterial activity of GA is enhanced in the presence of the released ions. Thus, by using smaller doses of drug the antibacterial effect can be maximized, while its toxic effects could be minimized. Further investigations are required to confirm these results with other bacterial strains.

4. Conclusions

In the first part of this study, MBGNs in the SiO_2-P_2O_5(B_2O_3)-CaO-Na_2O(MgO/ZnO) compositional system were successfully synthesized via a microemulsion assisted sol-gel method. All samples had a typical glass structure, with no diffraction peaks recorded for B doped compositions. However, for S53P4 nanoparticles a poorly crystalline HA was identified. The ATR-FTIR spectra confirmed that phosphate groups were present in S53P4, while the other samples showed a typical borosilicate network. For all compositions, the nanoparticles had a spherical shape with a radial network of slit-shape mesopores. Moreover, for S53P4 nanoparticles a second fraction of particles richer in Ca and P with a smaller diameter and a more compact internal structure was identified. In the second part of this work, MBGNs were studied as GA nanocarriers. GA was loaded by physical adsorption with the highest loading efficiency achieved by

B+Mg. *In vitro* release studies revealed an initial burst release of GA, followed by a slower release in the next 21 h. Between 24 h and 10 days, GA was continuously and constantly released. The highest cumulative release was achieved for S53P4 sample, while the smallest value was recorded for B+Mg. The antibacterial assay against both *S. aureus* and *E. coli* confirmed a stronger antibacterial effect for Zn doped compositions compared to the other unloaded samples. The loading of GA into S53P4 and B+Zn samples led to a synergistical antibacterial effect. In the short term, MBGNs and GA-MBGNs were more effective against *S. aureus*, whereas for 24 h they were more effective against *E. coli*. Further cell viability studies and *in vitro* wound scratch assay should be carried out. These MBGNs could be used for the simultaneous and smart delivery of different drugs or as inorganic fillers in 3D printed hydrogel scaffolds.

Acknowledgments

The present study was carried out with the founds and facilities provided by the Institute of Biomaterials, University of Erlangen–Nuremberg (FAU). Authors would like to thank the Central Facilities of the Universidad de Sevilla (CITUS) for the use of the TEM.

References

[1] IDF Diabetes Atlas | Tenth Edition, (n.d.). https://diabetesatlas.org/ (accessed November 15, 2022).

[2] M. Jiang, F. Gan, M. Gan, H. Deng, X. Chen, X. Yuan, D. Huang, S. Liu, B. Qin, Y. Wei, S. Su, Z. Bo, Predicting the Risk of Diabetic Foot Ulcers From Diabetics With Dysmetabolism: A Retrospective Clinical Trial, Front. Endocrinol. (Lausanne). 13 (2022) 1447. https://doi.org/10.3389/FENDO.2022.929864/BIBTEX.

[3] J.A. Rubio, S. Jiménez, J.L. Lázaro-Martínez, Mortality in Patients with Diabetic Foot Ulcers: Causes, Risk Factors, and Their Association with Evolution and Severity of Ulcer, J. Clin. Med. 9 (2020) 1–14. https://doi.org/10.3390/JCM9093009.

[4] M. Edmonds, C. Manu, P. Vas, The current burden of diabetic foot disease, J. Clin. Orthop. Trauma. 17 (2021) 88. https://doi.org/10.1016/J.JCOT.2021.01.017.

[5] M. Vuorlaakso, J. Kiiski, T. Salonen, M. Karppelin, M. Helminen, I. Kaartinen, Major Amputation Profoundly Increases Mortality in Patients With Diabetic Foot Infection, Front. Surg. 8 (2021) 101. https://doi.org/10.3389/FSURG.2021.655902/BIBTEX.

[6] R.F. Pereira, P.J. Bártolo, Traditional Therapies for Skin Wound Healing, Adv. Wound Care. 5 (2016) 208. https://doi.org/10.1089/WOUND.2013.0506.

[7] T. Mehrabi, A.S. Mesgar, Z. Mohammadi, Bioactive Glasses: A Promising Therapeutic Ion Release Strategy for Enhancing Wound Healing, ACS Biomater. Sci. Eng. 6 (2020) 5399–5430. https://doi.org/10.1021/ACSBIOMATERIALS.0C00528/ASSET/IMAGES/LAR

GE/AB0C00528_0008.JPEG.

[8] Y. Pilehvar-Soltanahmadi, M. Dadashpour, A. Mohajeri, A. Fattahi, R. Sheervalilou, N. Zarghami, An Overview on Application of Natural Substances Incorporated with Electrospun Nanofibrous Scaffolds to Development of Innovative Wound Dressings, Mini-Reviews Med. Chem. 18 (2017) 414–427. https://doi.org/10.2174/1389557517666170308112147.

[9] P. Monika, M.N. Chandraprabha, A. Rangarajan, P.V. Waiker, K.N. Chidambara Murthy, Challenges in Healing Wound: Role of Complementary and Alternative Medicine, Front. Nutr. 8 (2022) 1198. https://doi.org/10.3389/FNUT.2021.791899/BIBTEX.

[10] M. Cannio, D. Bellucci, J.A. Roether, D.N. Boccaccini, V. Cannillo, Bioactive Glass Applications: A Literature Review of Human Clinical Trials, Mater. (Basel, Switzerland). 14 (2021). https://doi.org/10.3390/MA14185440.

[11] S. Hooshmand, S. Mollazadeh, N. Akrami, M. Ghanad, A. El-Fiqi, F. Baino, S. Nazarnezhad, S. Kargozar, Mesoporous Silica Nanoparticles and Mesoporous Bioactive Glasses for Wound Management: From Skin Regeneration to Cancer Therapy, Materials (Basel). 14 (2021) 3337. https://doi.org/10.3390/MA14123337.

[12] T. Mehrabi, A.S. Mesgar, Z. Mohammadi, Bioactive Glasses: A Promising Therapeutic Ion Release Strategy for Enhancing Wound Healing, ACS Biomater. Sci. Eng. 6 (2020) 5399–5430. https://doi.org/10.1021/ACSBIOMATERIALS.0C00528/ASSET/IMAGES/MEDIUM/AB0C00528_0009.GIF.

[13] S. Naseri, W.C. Lepry, S.N. Nazhat, Bioactive glasses in wound healing: hope or

hype?, J. Mater. Chem. B. 5 (2017) 6167–6174. https://doi.org/10.1039/C7TB01221G.

[14] C. Migneco, E. Fiume, E. Verné, F. Baino, A Guided Walk through the World of Mesoporous Bioactive Glasses (MBGs): Fundamentals, Processing, and Applications, Nanomaterials. 10 (2020). https://doi.org/10.3390/nano10122571.

[15] L.L. Hench, J.R. Jones, Bioactive glasses: Frontiers and Challenges, Front. Bioeng. Biotechnol. 3 (2015) 194. https://doi.org/10.3389/FBIOE.2015.00194/BIBTEX.

[16] P. Balasubramanian, T. Büttner, V. Miguez Pacheco, A.R. Boccaccini, Boron-containing bioactive glasses in bone and soft tissue engineering, J. Eur. Ceram. Soc. 38 (2018) 855–869. https://doi.org/10.1016/J.JEURCERAMSOC.2017.11.001.

[17] Q. Nawaz, M.A.U. Rehman, A. Burkovski, J. Schmidt, A.M. Beltrán, A. Shahid, N.K. Alber, W. Peukert, A.R. Boccaccini, Synthesis and characterization of manganese containing mesoporous bioactive glass nanoparticles for biomedical applications, J. Mater. Sci. Mater. Med. 29 (2018) 1–13. https://doi.org/10.1007/S10856-018-6070-4/TABLES/3.

[18] F. Westhauser, S. Wilkesmann, Q. Nawaz, S.I. Schmitz, A. Moghaddam, A.R. Boccaccini, Osteogenic properties of manganese-doped mesoporous bioactive glass nanoparticles, J. Biomed. Mater. Res. Part A. 108 (2020) 1806–1815. https://doi.org/10.1002/JBM.A.36945.

[19] S. Demirci, A. Doğan, S. Aydın, E.Ç. Dülger, F. Şahin, Boron promotes streptozotocin-induced diabetic wound healing: roles in cell proliferation and migration, growth factor expression, and inflammation, Mol. Cell. Biochem. 417 (2016) 119–133. https://doi.org/10.1007/S11010-016-2719-9.

[20] P. Balasubramanian, L. Hupa, B. Jokic, R. Detsch, A. Grünewald, A.R. Boccaccini, Angiogenic potential of boron-containing bioactive glasses: in vitro study, J. Mater. Sci. 52 (2017) 8785–8792. https://doi.org/10.1007/S10853-016-0563-7/FIGURES/5.

[21] D. Ege, K. Zheng, A.R. Boccaccini, Borate Bioactive Glasses (BBG): Bone Regeneration, Wound Healing Applications, and Future Directions, ACS Appl. Bio Mater. 5 (2022) 3608–3622. https://doi.org/10.1021/ACSABM.2C00384/ASSET/IMAGES/LARGE/MT2C00384_0011.JPEG.

[22] N. Zhao, D. Zhu, Endothelial responses of magnesium and other alloying elements in magnesium-based stent materials, Metallomics. 7 (2015) 118. https://doi.org/10.1039/C4MT00244J.

[23] Y. Sasaki, G.A. Sathi, O. Yamamoto, Wound healing effect of bioactive ion released from Mg-smectite, Mater. Sci. Eng. C. 77 (2017) 52–57. https://doi.org/10.1016/J.MSEC.2017.03.236.

[24] P.H. Lin, M. Sermersheim, H. Li, P.H.U. Lee, S.M. Steinberg, J. Ma, Zinc in Wound Healing Modulation, Nutrients. 10 (2018). https://doi.org/10.3390/NU10010016.

[25] S. Kargozar, M. Mozafari, S. Hamzehlou, F. Baino, Using Bioactive Glasses in the Management of Burns, Front. Bioeng. Biotechnol. 7 (2019) 62. https://doi.org/10.3389/FBIOE.2019.00062.

[26] M. Jarosz, M. Olbert, G. Wyszogrodzka, K. Młyniec, T. Librowski, Antioxidant and anti-inflammatory effects of zinc. Zinc-dependent NF-κB signaling, Inflammopharmacology. 25 (2017) 11. https://doi.org/10.1007/S10787-017-0309-

4.

[27] Zakaria Tabia, K.E. Mabrouk, Meriame Bricha, Khalid Nouneh, Mesoporous bioactive glass nanoparticles doped with magnesium: drug delivery and acellular in vitro bioactivity, RSC Adv. 9 (2019) 12232–12246. https://doi.org/10.1039/C9RA01133A.

[28] C. Migneco, E. Fiume, E. Verné, F. Baino, A guided walk through the world of mesoporous bioactive glasses (MBGs): Fundamentals, processing, and applications, Nanomaterials. 10 (2020) 1–26. https://doi.org/10.3390/nano10122571.

[29] J. Hum, A.R. Boccaccini, Bioactive glasses as carriers for bioactive molecules and therapeutic drugs: a review, J. Mater. Sci. Mater. Med. 2012 2310. 23 (2012) 2317–2333. https://doi.org/10.1007/S10856-012-4580-Z.

[30] T. Mehrabi, A.S. Mesgar, Z. Mohammadi, Bioactive Glasses: A Promising Therapeutic Ion Release Strategy for Enhancing Wound Healing, (2020). https://doi.org/10.1021/acsbiomaterials.0c00528.

[31] K. Yang, L. Zhang, P. Liao, Z. Xiao, F. Zhang, D. Sindaye, Z. Xin, C. Tan, J. Deng, Y. Yin, B. Deng, Impact of Gallic Acid on Gut Health: Focus on the Gut Microbiome, Immune Response, and Mechanisms of Action, Front. Immunol. 11 (2020) 2231. https://doi.org/10.3389/FIMMU.2020.580208/BIBTEX.

[32] Q. Nawaz, M. Fuentes-Chandía, V. Tharmalingam, M.A. Ur Rehman, A. Leal-Egaña, A.R. Boccaccini, Silibinin releasing mesoporous bioactive glass nanoparticles with potential for breast cancer therapy, Ceram. Int. 46 (2020) 29111–29119. https://doi.org/10.1016/J.CERAMINT.2020.08.083.

[33] K. Ilyas, L. Singer, M.A. Akhtar, C.P. Bourauel, A.R. Boccaccini, Boswellia sacra

Extract-Loaded Mesoporous Bioactive Glass Nano Particles: Synthesis and Biological Effects, Pharmaceutics. 14 (2022) 126. https://doi.org/10.3390/PHARMACEUTICS14010126.

[34] K. Schuhladen, J.A. Roether, A.R. Boccaccini, Bioactive glasses meet phytotherapeutics: The potential of natural herbal medicines to extend the functionality of bioactive glasses, Biomaterials. 217 (2019) 119288. https://doi.org/10.1016/J.BIOMATERIALS.2019.119288.

[35] B. Badhani, N. Sharma, R. Kakkar, Gallic acid: a versatile antioxidant with promising therapeutic and industrial applications, RSC Adv. 5 (2015) 27540–27557. https://doi.org/10.1039/C5RA01911G.

[36] Q.M. Tian, S.M. Wei, H.R. Su, S.M. Zheng, S.Y. Xu, M.J. Liu, R.N. Bo, J.G. Li, Bactericidal activity of gallic acid against multi-drug resistance Escherichia coli, Microb. Pathog. 173 (2022) 105824. https://doi.org/10.1016/J.MICPATH.2022.105824.

[37] J. Lee, K.H. Choi, J. Min, H.J. Kim, J.P. Jee, B.J. Park, Functionalized ZnO Nanoparticles with Gallic Acid for Antioxidant and Antibacterial Activity against Methicillin-Resistant S. aureus, Nanomater. (Basel, Switzerland). 7 (2017). https://doi.org/10.3390/NANO7110365.

[38] D.J. Yang, S.H. Moh, D.H. Son, S. You, A.W. Kinyua, C.M. Ko, M. Song, J. Yeo, Y.H. Choi, K.W. Kim, Gallic Acid Promotes Wound Healing in Normal and Hyperglucidic Conditions, Molecules. 21 (2016). https://doi.org/10.3390/MOLECULES21070899.

[39] A. Houaoui, I. Lyyra, R. Agniel, E. Pauthe, J. Massera, M. Boissière, Dissolution, bioactivity and osteogenic properties of composites based on polymer and silicate

or borosilicate bioactive glass, Mater. Sci. Eng. C. 107 (2020) 110340. https://doi.org/10.1016/J.MSEC.2019.110340.

[40] G. Kaur, O.P. Pandey, K. Singh, D. Homa, B. Scott, G. Pickrell, A review of bioactive glasses: Their structure, properties, fabrication and apatite formation, J. Biomed. Mater. Res. - Part A. 102 (2014) 254–274. https://doi.org/10.1002/JBM.A.34690.

[41] A.J. Salinas, P. Esbrit, Mesoporous Bioglasses Enriched with Bioactive Agents for Bone Repair, with a Special Highlight of María Vallet-Regí's Contribution, Pharmaceutics. 14 (2022). https://doi.org/10.3390/PHARMACEUTICS14010202.

[42] A.I. Damian-Buda, G. Voicu, B.S. Vasile, A. Banciu, F. Iordache, L.T. Ciocan, Development of mesoporous borosilicate bioactive glass nanoparticles containing Mg2+ and Zn2+: biocompatibility, bioactivity and antibacterial activity, J. Non. Cryst. Solids. 594 (2022). https://doi.org/10.1016/J.JNONCRYSOL.2022.121819.

[43] E. Pinho, G. Soares, M. Henriques, Cyclodextrin modulation of gallic acid in vitro antibacterial activity, (n.d.). https://doi.org/10.1007/s10847-014-0449-8.

[44] N. Mutlu, F. Kurtuldu, I. Unalan, Z. Neščáková, H. Kaňková, D. Galusková, M. Michálek, L. Liverani, D. Galusek, A.R. Boccaccini, Effect of Zn and Ga doping on bioactivity, degradation, and antibacterial properties of borate 1393-B3 bioactive glass, Ceram. Int. 48 (2022) 16404–16417. https://doi.org/10.1016/J.CERAMINT.2022.02.192.

[45] S. Novak, J.R. Orives, M. Nalin, I. Unalan, A.R. Boccaccini, E.R. de Camargo, Quaternary bioactive glass-derived powders presenting submicrometric particles and antimicrobial activity, Ceram. Int. 48 (2022) 29982–29990. https://doi.org/10.1016/J.CERAMINT.2022.06.266.

[46] Q. Nawaz, M.A.U. Rehman, A. Burkovski, J. Schmidt, A.M. Beltrán, A. Shahid, N.K. Alber, W. Peukert, A.R. Boccaccini, Synthesis and characterization of manganese containing mesoporous bioactive glass nanoparticles for biomedical applications, J. Mater. Sci. Mater. Med. 29 (2018). https://doi.org/10.1007/s10856-018-6070-4.

[47] K. Zheng, Y. Fan, E. Torre, P. Balasubramanian, N. Taccardi, C. Cassinelli, M. Morra, G. Iviglia, A.R. Boccaccini, Incorporation of Boron in Mesoporous Bioactive Glass Nanoparticles Reduces Inflammatory Response and Delays Osteogenic Differentiation, Part. Part. Syst. Charact. 37 (2020) 2000054. https://doi.org/10.1002/PPSC.202000054.

[48] K. Zheng, A. Solodovnyk, W. Li, O.-M. Goudouri, C. Stähli, S.N. Nazhat, A.R. Boccaccini, Aging Time and Temperature Effects on the Structure and Bioactivity of Gel-Derived 45S5 Glass-Ceramics, J. Am. Ceram. Soc. 98 (2015) 30–38. https://doi.org/10.1111/jace.13258.

[49] X.V. Bui, T.H. Dang, Bioactive glass 58S prepared using an innovation sol-gel process, Process. Appl. Ceram. 13 (2019) 98–103. https://doi.org/10.2298/PAC1901098B.

[50] G. Shao, X. Wu, Y. Kong, S. Cui, X. Shen, C. Jiao, J. Jiao, Thermal shock behavior and infrared radiation property of integrative insulations consisting of MoSi2/borosilicate glass coating and fibrous ZrO2 ceramic substrate, Surf. Coatings Technol. 270 (2015) 154–163. https://doi.org/10.1016/J.SURFCOAT.2015.03.008.

[51] F. Kurtuldu, N. Mutlu, M. Michálek, K. Zheng, M. Masar, L. Liverani, S. Chen, D. Galusek, A.R. Boccaccini, Cerium and gallium containing mesoporous

bioactive glass nanoparticles for bone regeneration: Bioactivity, biocompatibility and antibacterial activity, Mater. Sci. Eng. C. 124 (2021). https://doi.org/10.1016/J.MSEC.2021.112050.

[52] M. V. Nikolenko, K. V. Vasylenko, V.D. Myrhorodska, A. Kostyniuk, B. Likozar, Synthesis of Calcium Orthophosphates by Chemical Precipitation in Aqueous Solutions: The Effect of the Acidity, Ca/P Molar Ratio, and Temperature on the Phase Composition and Solubility of Precipitates, Process. 2020, Vol. 8, Page 1009. 8 (2020) 1009. https://doi.org/10.3390/PR8091009.

[53] D.J. Yang, S.H. Moh, D.H. Son, S. You, A.W. Kinyua, C.M. Ko, M. Song, J. Yeo, Y.H. Choi, K.W. Kim, Gallic Acid Promotes Wound Healing in Normal and Hyperglucidic Conditions, Molecules. 21 (2016). https://doi.org/10.3390/MOLECULES21070899.

[54] A.C. Mera, D. Contreras, N. Escalona, H.D. Mansilla, BiOI microspheres for photocatalytic degradation of gallic acid, J. Photochem. Photobiol. A Chem. 318 (2016) 71–76. https://doi.org/10.1016/j.jphotochem.2015.12.005.

[55] V.S. Fedenko, M. Landi, S.A. Shemet, Metallophenolomics: A Novel Integrated Approach to Study Complexation of Plant Phenolics with Metal/Metalloid Ions, Int. J. Mol. Sci. 2022, Vol. 23, Page 11370. 23 (2022) 11370. https://doi.org/10.3390/IJMS231911370.

[56] S. Iraji, F. Ganji, L. Rashidi, Surface modified mesoporous silica nanoparticles as sustained-release gallic acid nano-carriers, J. Drug Deliv. Sci. Technol. 47 (2018) 468–476. https://doi.org/10.1016/J.JDDST.2018.08.008.

[57] G. Petrisor, D. Ficai, L. Motelica, R.D. Trusca, A.C. Bîrcă, B.S. Vasile, G. Voicu, O.C. Oprea, A. Semenescu, A. Ficai, M.I. Popitiu, I. Fierascu, R.C. Fierascu, E.L.

Radu, L. Matei, L.D. Dragu, I.M. Pitica, M. Economescu, C. Bleotu, Mesoporous Silica Materials Loaded with Gallic Acid with Antimicrobial Potential, Nanomater. 2022, Vol. 12, Page 1648. 12 (2022) 1648. https://doi.org/10.3390/NANO12101648.

[58] İ. Gulcin, S.H. Alwasel, Metal Ions, Metal Chelators and Metal Chelating Assay as Antioxidant Method, Process. 2022, Vol. 10, Page 132. 10 (2022) 132. https://doi.org/10.3390/PR10010132.

[59] A. Borges, C. Ferreira, M.J. Saavedra, M. Simões, Antibacterial activity and mode of action of ferulic and gallic acids against pathogenic bacteria, Microb. Drug Resist. 19 (2013) 256–265. https://doi.org/10.1089/MDR.2012.0244.

Figure Captions

Fig. 1 (a) XRD patterns and (b) ATR-FTIR spectra of MBGNs.

Fig. 2 SEM images of (a1) S53P4, (b1) B+Mg, (c1) B+Zn and (d1) B+Mg+Zn. TEM images and EDX spectra of (a2) S53P4, (b2) B+Mg, (c2) B+Zn and (d2) B+Mg+Zn. Numbered weighted density distribution for (a3) S53P4, (b3) B+Mg, (c3) B+Zn and (d3) B+Mg+Zn.

Fig. 3 STEM image with the corresponding EDX mapping of elements for S53P4 MBGNs.

Fig. 4 Optimization of drug loading for (a) S53P4, (b) B+Mg, (c) B+Zn and (d) B+Mg+Zn MBGNs.

Fig. 5 *In vitro* drug release study up to (a) 30 h and (b) 10 days. (c) Schematic representation of the possible drug release mechanism.

Fig. 6 *In vitro* antibacterial activity of MBGNs against (a) *E. coli* and (b) *S. aureus*.

Declaration of interests

☒ The authors declare that they have no known competing financial interests or personal relationships that could have appeared to influence the work reported in this paper.

☐The authors declare the following financial interests/personal relationships which may be considered as potential competing interests: